Main Manuscript for

SLC35G3 is a UDP-N-acetylglucosamine transporter for sperm glycoprotein formation and underpins male fertility in mice

Authors:

Daisuke Mashiko[1,2], Shingo Tonai[1], Haruhiko Miyata[1], Martin M. Matzuk[3,4], and *Masahito Ikawa[1, 2, 5, 6,7]

Affiliation:

1. Department of Experimental Genome Research, Research Institute for Microbial Diseases, Osaka University, Suita, Osaka 565-0871, Japan;
2. Immunology Frontier Research Center, Osaka University, Suita, Osaka 565-0871, Japan
3. Department of Pathology and Immunology, Baylor College of Medicine, Houston, TX 77030.
4. Center for Drug Discovery, Baylor College of Medicine, Houston, TX 77030.
5. Center for Advanced Modalities and Drug Delivery System, Osaka University, Osaka 565-0871, Japan
6. Center for Infectious Disease Education and Research, Osaka University, Osaka 565-0871, Japan
7. The Institute of Medical Science, The University of Tokyo, Minato-ku, Tokyo 108-8639, Japan.

***Corresponding author. Email: ikawa@biken.osaka-u.ac.jp**

Author Contributions: Conceptualization: DM, MMM, and MI. Data curation: DM. Formal analysis: DM. Funding acquisition: HM, MMM and MI. Methodology: DM, HM, MMM, and MI. Project administration: MI. Investigation: DM, ST, HM, and MI. Visualization: DM, HM, and MMM. Supervision: MI. Writing—original draft: DM and MI. Writing—review & editing: All authors

Competing Interest Statement: The authors declare no conflict of interest.

Classification: Biological Sciences, Developmental Biology.

Keywords: Zona pellucida binding, Utero tubal junction penetration, Sterility

This file includes:

Main Text

Figures 1 to 7

Abstract

Despite the recognized importance of glycans in biological phenomena, their complex roles in spermatogenesis and sperm function remain unclear. SLC35G3, a 10-transmembrane protein specifically found in early round spermatids, belongs to the sugar-nucleotide transporter family, indicating its involvement in glycan formation. In this study, we found that *Slc35g3* knockout male mice were sterile due to impaired sperm functions in uterotubal junction passage, zona pellucida binding, and oocyte fusion. Mouse SLC35G3 has UDP-GlcNAc transporter activity, and its ablation caused abnormal processing of the sperm plasma membrane and acrosome membrane proteins. Reported human *SLC35G3* mutations (F267L and T179HfsTer27) diminished the UDP-GlcNAc transporter activity of SLC35G3, implying infertility risks in males carrying these mutations. Our findings unveil the vital roles of SLC35G3 in the glycan formation of sperm membrane proteins critical for sperm fertilizing ability.

Introduction

Glycosylation is a post-translational modification that ensures target protein synthesis, secretion, stability, characterization, and/or function (1-3). In the endoplasmic reticulum (ER), the oligosaccharyltransferase complex (OSTC) co-translationally transfers core glycans assembled on dolichol phosphate to asparagine residues of nascent proteins. Subsequently, these proteins undergo a quality control process in which the core glycan structure is processed by glucosidases, resulting in a monoglucosylated form that binds to ER lectin chaperones, calnexin (CANX) and calreticulin (CALR). Once disulfide bonds are correctly formed by protein disulfide isomerase (PDI) and the protein is properly folded, the protein is transported to the Golgi (4, 5). Notably, there are testis-specific proteins that are required for these processes and the regulation of sperm fertilizing ability. Recent studies suggest that FREY tightly interacts with proteins involved in N-glycosylation, and its disruption destabilizes OSTC and causes subsequent ablation of the acrosomal membrane proteins essential for sperm-egg fusion (6, 7). In addition to the CANX/CALR/PDI complex in somatic cells, their testis-specific paralogs, CLGN/CALR3/PDILT, are required for ADAM3 sperm membrane glycoprotein maturation to equip sperm with fertilization competence, including the ability to pass through the uterotubal junction (UTJ) (8).

In the ER to Golgi secretory pathway, more than 200 glycosyltransferases, such as mannosyl (alpha-1,3-)-glycoprotein beta-1,2-N-acetylglucosaminyltransferase (MGAT) and N-acetylgalactosaminyltransferase (GALNT), add further diversity by conferring various properties, such as solubility and adhesiveness to the proteins. Once glycoproteins reach the cell surface, some are secreted to form the extracellular matrix, while others remain and contribute to cell adhesion and interactions with substrates or other cells. Among these glycosyltransferase-like proteins, DPY19L2 (a probable C-mannosyltransferase), MGAT4D, MGAT4E, MGAT4F, and GALNTL5 show testis-specific expression by *in silico* analysis (9). *Dpy19l2* knockout mice are infertile due to globozoospermia (10), and a mutation in *Galntl5* resulted in asthenozoospermia (11). Of note, GALNTL5 does not exhibit transferase activity *in vitro* (12). While *Mgat4d* knockout mice are fertile (13), *Mgat4e* and *Mgat4f* orthologs do not exist in humans, and their knockout mice need to be generated to reveal if they have indispensable or redundant functions in mice. Collectively, these findings suggest that the spermatogenic cells have a unique system for the production and quality control of glycoproteins, and some of them are critical for spermatogenesis, sperm functions, and male fertility.

In the present study, we focused on the solute carrier (SLC) 35 family of nucleotide sugar transporters, which are responsible for importing sugars that serve as substrates for glycosyltransferases. Sugars are conjugated to nucleotides and transported by specific SLC35 family antiporters into the ER and Golgi apparatus, where glycosyltransferases utilize them to modify target proteins. Glycan structures are synthesized from sugars including D-glucose (Glc), D-galactose (Gal), N-acetyl-D-glucosamine (GlcNAc), N-acetyl-D-galactosamine (GalNAc), L-fucose (Fuc), D-glucuronic acid (GlcA), D-mannose (Man), N-acetylneuraminic acid (Neu), and D-xylose (Xyl). Among the SLC35 paralogs, SLC35A1 transports CMP-Sialic Acid, SLC35A2 transports UDP-Gal, SLC35B4 transports UDP-GlcNAc, and SLC35C1 transports GDP-Fuc (14). Of the 27 SLC35 family members, most show ubiquitous expressions, including in spermatogenic cells. Notably, in silico analysis revealed that *Slc35g3* is the only SLC35 family member specifically expressed in the testis. *Slc35g3* emerged in amphibians and is conserved in primates. We elucidated the biochemical properties of SLC35G3 *in vitro* and generated *Slc35g3* knockout mice to study its physiological functions *in vivo*. We discovered that SLC35G3 is a spermatogenic cell-specific UDP-GlcNAc transporter, and *Slc35g3* ablation results in abnormal processing of sperm plasma membrane and acrosome membrane glycoproteins required for sperm fertilizing ability and male fertility.

Results

SLC35G3 is expressed during late spermatogenesis and localized in the Golgi apparatus

In mice, *Slc35g3* comprises two coding exons and is located on chromosome 11, whereas it is located on chromosome 17 in humans. The TreeFam (15) data confirmed the evolutionary conservation of *Slc35g3* among vertebrates (**Fig. 1A**). RT-PCR analysis indicates that it is prominently expressed in the testis, beginning 21 days postpartum (**Fig. 1B**), suggesting that its expression begins in round spermatids in mice. The Mammalian Reproductive Genetics Database (16) revealed that *Slc35g3* is the only mouse SLC35 family that shows a testis-specific transcription pattern (**Fig. S1**). A previous scRNA-seq analysis suggested that transcription of *Slc35g3* initiates in round spermatids (**Fig. 1C;** Mouse Cell Atlas; 17). Both AlphaFold2 (18) and TOPCONS (19) analyses supported that SLC35G3 has 10 transmembrane domains (**Fig. 1D**), likely forming a homodimer (**Fig. S2**). Immunostaining colocalizes SLC35G3 with Golgi marker (GM) 130 (Golgin A2), indicating SLC35G3 localization in the Golgi of mouse testicular germ cells (**Fig. 1E**).

Slc35g3$^{-/-}$ mice showed male infertility

To investigate the roles of *Slc35g3* in male reproduction, we used CRISPR/Cas9 to generate a homozygous knockout mouse line (*Slc35g3*$^{-/-}$) with an 1804-bp deletion on a hybrid B6D2 background. This deletion resulted in the loss of the entire *Slc35g3* coding region (**Fig. 2A, 2B**), indicating that it should be a null allele.

Slc35g3$^{-/-}$ mice exhibit grossly normal development, appearance, and behavior, consistent with its testis-restricted expression. Absence of the *Slc35g3* mRNA and SLC35G3 protein in the *Slc35g3*$^{-/-}$ testes was verified by RNA-seq (**Fig. S3)** and western blot analysis (**Fig. 2C**), respectively. The specific expression of SLC35G3 in the testis, but not in epididymal sperm, suggests that its function is restricted to spermatogenesis. Moreover, immunofluorescence of SLC35G3 confirmed its absence in the Golgi of *Slc35g3*$^{-/-}$ mice (**Fig. S4**). Testes of *Slc35g3*$^{-/-}$ male mice appeared normal in both

appearance and weight (**Fig. 2D, 2E;** +/+ vs. -/-, two-sided Student's t-test; $\boldsymbol{P} = 0.42$). Despite successful copulation, as evidenced by the presence of vaginal plugs, *Slc35g3*$^{-/-}$ male mice are sterile (**Fig. 2F;** +/+ vs. -/-, two-sided Wilcoxon rank-sum test, $\boldsymbol{P} = 2.87 \times 10^{-10}$). Examination of seminiferous tubule and epididymis sections revealed no overt abnormalities **(Fig. 2G** and **Fig. S5**). Furthermore, computer-assisted sperm analysis revealed no significant differences in the motility of sperm from control and *Slc35g3*$^{-/-}$ males (**Fig. S6**).

Slc35g3$^{-/-}$ -derived sperm exhibit abnormal head morphology

Given the subtle morphological changes observed in *Slc35g3*$^{-/-}$-derived sperm (**Fig. 3A**), we employed elliptic Fourier descriptors (20, 21) to characterize the entire sperm head shape and conducted a principal component (PC) analysis (**Fig. 3B, 3C, 3D**). Wild-type-derived sperm and *Slc35g3*$^{-/-}$-derived sperm could be differentiated based on their PC2 analysis of the tip of the sperm heads, with *Slc35g3*$^{-/-}$-derived sperm displaying a relatively higher PC2 value (**Fig. 3C**), indicating the lack of the hook shape in *Slc35g3*$^{-/-}$ -derived sperm. The head shape of *Slc35g3*$^{-/-}$-derived sperm resembled that of sperm from *Fam71f2*$^{-/-}$ (recently renamed as *Garin1a*, Golgi-associated RAB2 interactor 1A)(22) mice (**Fig. S7**). However, *Slc35g3*$^{-/-}$ mice exhibited a more severe fertility phenotype compared to *Fam71f2*$^{-/-}$ mice (average litter size = 0 and 4.4 pups/litter, respectively), suggesting that sperm head morphology is not the sole cause of sterility in *Slc35g3*$^{-/-}$ mice.

Slc35g3$^{-/-}$-derived sperm exhibit impaired zona pellucida (ZP) binding and fertilization

To further analyze the cause of infertility in *Slc35g3* null male mice, we performed an in vitro fertilization (IVF) assay. We first performed conventional IVF using cumulus-intact oocytes with 2×10^5 sperm/mL insemination and found no oocytes fertilized with spermatozoa from *Slc35g3*$^{-/-}$ males (**Fig. 4A**). By removing cumulus cells followed by insemination (**Fig. 4B**), we found a decline in the number of *Slc35g3*$^{-/-}$-derived spermatozoa bound to the ZP (**Fig. 4C, 4D**), no oocytes fertilized as well (**Fig. 4E,** Wilcoxon rank-sum test; $\boldsymbol{P} = 0.0079$). Further study, using ZP-free oocytes preloaded with Hoechst33342 (**Fig. 4F**), revealed a significantly lower number of sperm fusing with the oocyte compared to control *Slc35g3*$^{+/-}$ (**Fig. 4G, H**, +/- vs. -/-, Wilcoxon rank-sum test, $\boldsymbol{P} = 1.71 \times 10^{-21}$). Notably, oolemma fusion and fertilization were improved with a 10 times higher sperm concentration from *Slc35g3*$^{-/-}$ males but were still significantly decreased compared to the lower concentrations of sperm from controls **(Fig. S8)**. Lastly, IVF performed using cumulus-intact oocytes with 10 times more sperm insemination (2×10^6 sperm/mL) resulted in a reduced fertilization rate (45.7%, 21/46), but we succeeded in obtaining 10 live pups from these fertilized eggs (**Fig. S9**). Our results indicate that *Slc35g3*$^{-/-}$-derived sperm have defects in ZP binding and oolemma fusion ability but produce viable offspring.

Slc35g3-deficient mice show impaired sperm migration to the oviduct.

As spermatozoa lacking ZP binding frequently cannot pass through the uterotubal junction (UTJ) and reach the oviduct (8), we observed sperm UTJ passage after mating. This observation was facilitated by a red fluorescence signal in the sperm tails from Tg mice (CAG/*su9*-DsRed2, *Acr3*-eGFP) (23; **Fig. 5A**). Two hours after copulation with wild-type female mice (**Fig. 5B**), control *Slc35g3*$^{+/-}$-derived sperm tail signals marked by red fluorescence were observed within the oviduct (**Fig. 5C**). In contrast, *Slc35g3*$^{-/-}$-

184 derived sperm were found in the uterus but not in the oviduct (**Fig. 5C**). Thus, the
185 defective UTJ migration is one of the primary causes of *Slc35g3*-/- male infertility.
186
187 ***Slc35g3* absence causes a reduced amount and abnormal processing of sperm**
188 **glycoproteins.**
189 To understand the molecular mechanisms behind the disrupted sperm functions
190 of *Slc35g3*$^{-/-}$ mice, we analyzed glycoproteins related to each process. First, we examined
191 proteins involved in acrosome formation. Immunoblot analysis of *Slc35g3*$^{+/+}$ and *Slc35g3*$^{-}$
192 $^{/-}$ testis lysates showed a reduction in the amount of ZP binding protein 1 (ZPBP1; 24),
193 whereas Golgi-associated PDZ and coiled-coil motif containing (GOPC; 25) levels
194 remained unchanged (**Fig. 6A**). Interestingly, SPACA1 (Sperm Acrosome Associated 1;
195 26) exhibited a subtle difference in banding pattern in the *Slc35g3*$^{-/-}$ testis lysate.
196 SPACA1 is N-glycosylated, and treatment of testis and caudal sperm lysates with
197 peptide-N-glycosidase F (PNGase F; **Fig. 6B, Fig. 6C**) resulted in comparable SPACA1
198 band patterns between *Slc35g3*$^{+/+}$ and *Slc35g3*$^{-/-}$ testes but not in sperm lysates. A similar
199 result was also reported in *Fam71f1* $^{-/-}$ (Garin1b; 22) mice, which exhibit abnormal
200 acrosome formation.
201 Next, we examined proteins involved in ZP binding. Levels of a disintegrin and
202 metalloprotease (ADAM) 1B (27) were comparable between *Slc35g3*$^{+/-}$ and *Slc35g3*$^{-/-}$ in
203 the testis (**Fig. 6D**) and sperm (**Fig. 6E**). Levels of CKLF-like MARVEL transmembrane
204 domain containing (CMTM) 2A and CMTM2B (28) were reduced in *Slc35g3*$^{-/-}$ testis
205 lysates but not in sperm. The expression pattern of ADAM3 (29, 30) was comparable
206 between *Slc35g3*$^{+/-}$ and *Slc35g3*$^{-/-}$ testis, yet the amount of a smaller isoform was elevated
207 in *Slc35g3*$^{-/-}$-derived sperm lysates, indicating aberrant processing. After PNGaseF
208 treatment of proteins, the ADAM3 band pattern was comparable between *Slc35g3*$^{+/-}$ and
209 *Slc35g3*$^{-/-}$ (**Fig. S10**). Given the aberrant ADAM3 band pattern was also observed in testis
210 expressed gene 101 (TEX101) knockout (31) epididymal caput sperm, we examined
211 TEX101 levels through western blot analysis; however, the amount of TEX101 was
212 comparable between *Slc35g3*$^{+/-}$ and *Slc35g3*$^{-/-}$ testis lysates (**Fig. 6D**). Given that the
213 testicular *Ace*$^{-/-}$ (t-ACE; 32, 33, 34) caused aberrant localization of ADAM3, we
214 examined t-ACE levels through western blot analysis and found that the amount of t-
215 ACE was comparable between *Slc35g3*$^{+/-}$ and *Slc35g3*$^{-/-}$ in both testis and sperm lysates
216 (**Fig. 6D, 6E**). In the previous studies, lymphocyte antigen 6 family member K (*Ly6k*)$^{-/-}$
217 (35), *Spaca4*$^{-/-}$ (36), and LY6/PLAUR Domain Containing 4 (*Lypd4*)$^{-/-}$ (37) sperm showed
218 impaired ZP binding; however, the amount of ADAM3 remained normal. The amount of
219 LY6K was reduced in *Slc35g3*$^{-/-}$ testis lysates (**Fig. 6D**), and the amount of SPACA4 was
220 comparable between *Slc35g3*$^{+/-}$ and *Slc35g3*$^{-/-}$ in both testis and sperm lysates (**Fig. 6D,**
221 **6E**). However, the amount of LYPD4 in *Slc35g3*$^{-/-}$ testis lysates decreased, and the lower
222 molecular weight band disappeared in *Slc35g3*$^{-/-}$-derived sperm lysates (**Fig. 6E**),
223 indicating the occurrence of a protein processing error or another non-N-linked
224 oligosaccharide post-translational defect.
225 Finally, we focused on the inner acrosomal membrane proteins involved in
226 oolemma fusion. IZUMO1 is an N-glycosylated acrosome membrane protein, and the
227 first to be identified as essential for sperm-oolemma fusion using knockout mice (38).
228 The levels of IZUMO1 decreased in both the testis and sperm of *Slc35g3*$^{-/-}$ mice.
229 Although the amount of IZUMO1 in sperm was less, we did not see any other bands in
230 the western blot analysis. IZUMO1 could relocate to the equatorial segment where fusion
231 occurs after the acrosome reaction in *Slc35g3*$^{-/-}$ derived spermatozoa (**Fig. S11**).
232 Equatorin (EQTN) is an O-linked glycosylated protein on the inner acrosomal membrane,

233 not essential for oolemma fusion but rather functions in oolemma binding. The EQTN
234 signal showed no difference between *Slc35g3*$^{+/-}$ and *Slc35g3*$^{-/-}$ testes, but it disappeared in
235 *Slc35g3*$^{-/-}$-derived sperm. Intriguingly, mass spectrometry analysis of sperm lysates
236 showed comparable quantitative values of EQTN between *Slc35g3*$^{+/-}$ and *Slc35g3*$^{-/-}$ mice
237 (**Table S1**). With the fact that the anti-EQTN antibody MN9 recognizes both peptide and
238 glycan structures and that the glycan structure (39), our data suggests that EQTN
239 glycosylation is aberrant in *Slc35g3*$^{-/-}$-derived sperm. SPACA6 is known to be lost from
240 all the sperm-oolemma fusion defective sperm (i.e., *Dcst1/2*, *Fimp*, *Izumo1*, *Sof1*,
241 *Spaca6*, and *Tmem95* knockout models) (40); however, we did not see any difference in
242 the intensity and band pattern using western blot analysis.
243
244 ***Slc35g3*$^{-/-}$-derived spermatozoa show impaired glycan structures**
245 To analyze the protein glycosylation status during spermatogenesis, we
246 performed lectin blot analyses using testis lysates (**Fig.7A**). The band patterns of
247 concanavalin A (ConA; detecting mannose), *Aleuria aurantia* lectin (AAL; detecting
248 fucose), and *Maackia amurensis* II (MAL-II; detecting sialic acid + core1 structure) were
249 comparable between *Slc35g3*$^{+/+}$ and *Slc35g3*$^{-/-}$ samples. Notably, with PNA, which detects
250 galactose β1-3 acetyl galactosamine (core 1 structure), the intensity of a band around 60
251 kDa increased in *Slc35g3*$^{-/-}$ testis. As PNA binding is known to be inhibited by any
252 galactose modifications (41), the core 1 modifications might be disrupted in the target
253 protein. With *Laetiporus sulphureus* lectin N-terminal domain (LSL-N; detecting
254 LacNAc: galactose-GlcNAc), signal intensities for small proteins decreased. Intriguingly,
255 the difference became evident when we performed lectin blot analysis using mature
256 spermatozoa. Some major signals disappeared in PNA and LSL-N blot analysis (**Fig.
257 7B**).
258
259 **Mouse (m) *Slc35g3* overexpression restored glycan levels in HEK293T cells without
260 human (h) *SLC35B4***
261 To investigate whether SLC35G3 acts as a UDP-GlcNAc transporter, we
262 performed rescue experiments with HEK293T cells. First, we designed two gRNAs to
263 knock out *hSLC35B4* encoding a known UDP-N-acetylglucosamine (UDP-GlcNAc)
264 transporter that is highly expressed in HEK293T cells (**Fig. S12A**). The *hSLC35B4*
265 knockout cells were obtained by transfecting pX459 containing two gRNAs and a
266 puromycin-resistant cassette, followed by puromycin treatment (**Fig. S12B**). After three
267 passages, the cells were transfected with a plasmid expressing *mSlc35b2* (encoding a
268 phosphoadenosine phosphosulfate transporter), *mSlc35b4*, or *mSlc35g3*-mCherry. We
269 found that the introduction of *mSlc35b2* did not rescue the amounts of proteins with
270 GlcNAc modification (**Fig. 7C**). Conversely, transfection with the *mSlc35b4*-expressing
271 plasmid rescued GlcNAc modification levels. Further, the LSL-N signals were rescued
272 by *mSlc35g3* transfection (**Fig. 7C**), suggesting that mSLC35G3 functions as a UDP-
273 GlcNAc transporter.
274
275 **T179HfsTer27 and F267L mutants failed to rescue glycan loss in *hSLC35B4*-
276 disrupted cells**
277 Among the frameshift mutations found in human genomes (n= 76156, gnomAD;
278 42), the T179HfsTer27 frame mutation has a relatively high allele frequency (1.88e^{-3}),
279 and homozygous mutations are observed in 54 individuals (29 females and 25
280 males). Moreover, AlphaMissense (43), a deep learning model trained on protein
281 sequences and annotations of pathogenicity, predicted 35 pathogenic missense mutations
282 in the *hSLC35G3* gene. Among these, two mutations (F215L and F267L) were identified

283 in human genomes, and we focused on F267L, which showed potential detrimental
284 effects according to the evolutionary conservation and protein 3D structure (PolyPhen-2;
285 44). PCR and subsequent direct sequencing confirmed that the *hSLC35G3* expression
286 plasmid (wild-type, FS, or F267L) was introduced into *hSLC35B4*$^{-/-}$ cells. With lectin blot
287 analysis using LSL-N, the signal decreased by *hSLC35B4*$^{-/-}$ was rescued by the
288 introduction of wild-type *hSLC35G3*, while no signal recovery was observed upon the
289 introduction of FS or F267L (**Fig. 7D**). The band patterns of ConA modification
290 remained consistent across all transfected cells. These findings suggest a loss of function
291 in the T179HfsTer27 and F267L mutations.
292
293 **Discussion**
294 In this study, we identified SLC35G3 as a testis-specific UDP-GlcNAc
295 transporter to underpin proper sperm glycoprotein synthesis and functions. Although
296 *Slc35g3*$^{-/-}$ male mice are viable, healthy, and produce motile sperm, they are completely
297 infertile, revealing a critical and unique role of SLC35G3 for producing functional
298 spermatozoa and male fertility. In vitro studies further implicated latent male infertility
299 due to *SLC35G3* mutations.
300 During spermatogenesis, *Slc35b4* is expressed in earlier stages, but it decreases
301 and is replaced by *Slc35g3* in later stages (**Fig. S1**). The reason for the stage-dependent
302 usage of two transporters is unknown, but it may be related to the formation of
303 acrosomes, which are rich in glycosylated proteins, in the later stages of spermatogenesis.
304 Although our in vitro data showed no clear differences (**Fig.7C**), SLC35B4 and
305 SLC35G3 may have different activities and/or functions. Alternatively, SLC35G3 may
306 have a lower optimal temperature because spermatogenesis progresses at a lower
307 temperature (45). Considering the transcript level of *Slc35g3* in later spermatogenesis
308 stages (highest TPM=320 at round spermatid) is higher than that of *Slc35b4* in the earlier
309 stage (highest TPM=21 at spermatogonia), spermatids may simply require more UDP-
310 GlcNAc transporter activity. Further in vitro and in vivo studies will be needed to answer
311 these questions, including transgenic mice expressing *Slc35b4* under the *Slc35g3*
312 promoter and vice versa. The answer will also help us to understand why and how
313 spermatogenic cells require a certain number of paralogous genes to be expressed
314 specifically.
315 Lectin blot analyses revealed no differences in ConA signals targeting terminal
316 mannose (**Fig. 7B**), indicating the normal formation of high-mannose-type
317 oligosaccharides for N-glycan biosynthesis in the ER of *Slc35g3*$^{-/-}$ spermatogenic cells
318 (46). For O-glycans, there was an increase in PNA signals (core 1, Gal-GalNAc) and a
319 reduction in LSL-N signals (LacNAc: Gal-GlcNAc), while no changes were observed for
320 MAL-II (sialic acid) and AAL (fucose). These findings suggest that SLC35G3 plays
321 a more important role in glycan elongation rather than core structure, and the impaired
322 elongated glycan structure affected the properties of glycoproteins and following sperm
323 morphology and functions in *Slc35g3*$^{-/-}$ mice.
324 While spermatogenesis looked grossly normal in *Slc35g3*$^{-/-}$ mice (**Fig. 2D, 2E,**
325 **and 2G, fig. S6**), their spermatozoa displayed multiple phenotypic abnormalities in head
326 morphology (**Fig. 3**), UTJ migration (**Fig. 5**), and fertilization (**Fig. 4**). Regarding sperm
327 head malformation, while globozoospermia results in male infertility (e.g., *Zpbp1* (24),
328 *Gopc* (25), and *Spaca1* (26) knockout mice), most of the knockout mice with only subtle
329 head malformation can produce offspring, although at lower levels (e.g., *Zpbp2* (24),
330 *Fam71f2* (22), and *Garin2-Garin5* (47) knockout mice). We found a subtle sperm head
331 malformation in *Slc35g3*$^{-/-}$ mice, but it should not be underestimated. For example, it has

332 been shown that mutations in multiple genes synergistically worsen head morphology,
333 even in the heterozygous state (48). Although we are still far from unraveling these
334 molecular interactions, we have revealed the importance of SLC35G3-mediated UDP-
335 GlcNAc transport for ZPBP1 stabilization and SPACA1 processing. While these proteins
336 are also found in humans, it is still too early to infer the importance of SLC35G3 in the
337 morphogenesis of human sperm heads. Observing sperm samples from individuals with
338 SLC35G3 mutations would be the most direct approach to address this, and we consider
339 it an important objective for future studies.
340 *Slc35g3*$^{-/-}$-derived spermatozoa exhibited defective UTJ passage (**Fig. 5**) and ZP
341 binding (**Fig. 4D**). These defects are commonly linked and observed in many infertile
342 knockout mice, and ADAM3 is absent from most of these knockout spermatozoa (37,
343 49). However, ADAM3 is present in the *Slc35g3*$^{-/-}$-derived spermatozoa as in four other
344 knockout mouse lines that show the same phenotype (i.e., *Ly6k, Pgap1, Spaca4*, and
345 *Lypd4* knockout lines). These results suggest that ADAM3 may be dysfunctional in these
346 mutant sperm, or that there may be an unknown factor responsible for UTJ passage and
347 ZP binding. Because LY6K and PGAP1 only function in the testis and disappear from
348 mature spermatozoa, we analyzed the presence of LYPD4 and SPACA4 in mature
349 spermatozoa and found that there was abnormal processing of LYPD4 in *Slc35g3*$^{-/-}$-
350 derived spermatozoa (**Fig. 6E**) compared to WT sperm (50). Since ADAM3 is no longer
351 active in humans, more attention needs to be paid to LYPD4 to understand the sperm
352 fertilizing ability.
353 We next focused on the inner acrosomal membrane proteins because *Slc35g3*$^{-/-}$
354 derived spermatozoa were defective in fusing with oocytes (**Fig. 6D, 6E**). While we did
355 not see any differences in SPACA6 western blot analysis, we found a decrease in
356 IZUMO1 in *Slc35g3*$^{-/-}$-derived spermatozoa, which is consistent with our previous study
357 showing the lack of glycosylation accompanied by a decrease in IZUMO1 levels and a
358 reduction in the number of pups (51). Intriguingly, while EQTN was detected by MS
359 analysis (**Table S1**), signals disappeared in our western blot analysis using an antibody
360 recognizing EQTN O-glycans (37; **Fig. 6E**), suggesting the presence of EQTN protein
361 without O-glycans. As *Eqtn* knockout spermatozoa decreased their oolemma binding
362 ability (37), EQTN glycans may directly contribute to oolemma binding. These results
363 suggest that SLC35G3 regulates sperm-oolemma fusion through O-linked glycosylation
364 of inner acrosomal membrane proteins.
365 Finally, we examined mutations in human *SLC35G3* for their potential risk of
366 male infertility. An in vitro study revealed that the T179HfsTer27 (17-35193772-GT-G)
367 mutation lost sugar-nucleotide transporter activity. According to gnomAD, its frequency
368 is $1.88 \times 10^{-3,}$ and 54 individuals have been identified as homozygous. In addition, the
369 observed/expected ratio of single-nucleotide variants causing loss of function was 0.53,
370 suggesting the presence of selective pressure due to mutations. Assessment of their sperm
371 fertilizing ability would be beneficial to understanding glycosylated protein synthesis and
372 functions in human spermatozoa. Even if the mutation caused male infertility, as we
373 obtained healthy offspring by IVF with higher concentration sperm insemination,
374 intracytoplasmic sperm injection might not be necessary for their treatment.
375 In conclusion, our research suggests that SLC35G3 functions as a testis-specific
376 UDP-GlcNAc transporter during late spermatogenesis. We reaffirmed that glycosylation-
377 related genes specific to the testis play a crucial role in the synthesis, quality control, and
378 function of glycoproteins on sperm, which are essential for male fertility through their
379 interactions with eggs and the female reproductive system. Furthermore, we
380 demonstrated that human SLC35G3 also exhibits transporter activity, and proposed a

loss-of-function mutation that may cause male infertility. Further research on this gene and sperm glycoprotein synthesis has the potential to contribute to understanding the causes of male infertility, developing treatments, and advancing contraceptive methods.

Methods

Experimental design

In this study, we developed an integrated approach, combining *in silico* analysis with experimental techniques, to elucidate the functions of SLC35G3. To generate *Slc35g3* knockout (*Slc35g3*$^{-/-}$) male mice, we used the CRISPR/Cas9 system and conducted *in silico* analysis for off-target/cleavage activity. Male fertility assessment encompasses mating with females, alongside IVF assays. Based on the preliminary literature on the SLC35 family, SLC35G3 is hypothesized to be a nucleotide sugar transporter. Therefore, we performed lectin blot analysis using tissue lysate/HEK293T cell lysate.

Animals

The manuscript adhered to the ARRIVE guidelines 2.0 for reporting. This study was performed following the standards outlined in the Guide for the Care and Use of Laboratory Animals. All animal experiments were approved by the Animal Care and Use Committee of the Research Institute for Microbial Diseases at Osaka University, Osaka, Japan (#Biken-AP-H30-01). The mice used in the study were sourced from Japan SLC, Inc. (Shizuoka, JP) and were bred under specific pathogen-free conditions. They were housed at 23°C, with a relative humidity of 50%, and a 12-h dark/12-h light cycle, with unrestricted access to water and commercial food pellets *ad libitum*. All genetically modified mice produced in this study will be accessible through either the RIKEN BioResource Research Center in Ibaraki, Japan, or the Center for Animal Resources and Development (CARD) at Kumamoto University, Japan.

In silico analysis

Phylogenetic tree analysis was performed using TreeFam (15; http://www.treefam.org/), while the Mammalian Reproductive Genetics Database (16; https://orit.research.bcm.edu/MRGDv2) was used for mRNA expression analysis of the SLC35 family. Previously reported single-cell RNA sequencing data (17; https://bis.zju.edu.cn/MCA/) were employed to analyze *Slc35g3* mRNA expression in testicular germ cells. The AlphaFold database (18; https://alphafold.ebi.ac.uk/) was utilized for structure prediction, and TOPCONS (19; https://topcons.cbr.su.se/) was employed for the topological analysis of SLC35G3.

RNA isolation and reverse transcription polymerase chain reaction

RNA was extracted and purified from various adult tissues of C57BL/6N mice at different stages using TRIzol reagent (Cat. No. 15596018, Thermo Fisher Scientific, Waltham, MA, USA), according to the manufacturer's instructions. Reverse transcription was conducted with the RNA using the SuperScript III First-Strand Synthesis System (Cat. No. 18080051; Thermo Fisher Scientific). PCR amplification was performed using a KOD Fx Neo (KFX-201; TOYOBO Co., LTD, Osaka, JP). The primer sequences used for each gene are listed in **Table S2**.

Visualization using fluorescence

429 Preparation of spermatogenic cells was performed as previously described for
430 testicular cells (52). Briefly, the seminiferous tubules were cut into small pieces, and the
431 contents were extracted by pressing them against a coverslip and frozen. Hoechst33342
432 (H3570, Thermo Fisher Scientific) and Alexa Fluor 568-conjugated peanut agglutinin
433 (PNA; L32458, Thermo Fisher Scientific) were used to stain the nuclei and acrosomes of
434 cauda epididymal spermatozoa. Observations were performed using a fluorescence
435 microscope (BX53; Olympus, Tokyo, JP).
436
437 **Generation of *Slc35g3* knockout mice**
438 *Slc35g3* knockout mice were generated using the CRISPR/Cas9 system. Guide
439 RNA design and potential off-target analysis were performed using the software
440 programs CRISPRdirect (https://crispr.dbcls.jp/) and CRISPOR
441 (https://crispor.tefor.net/). Fertilized eggs were obtained from the oviducts of super-
442 ovulated B6D2F1 females, which were then mated with BDF1 males. Ribonucleoprotein
443 (RNP) complexes, comprising synthesized CRISPR RNA (crRNA), trans-activating
444 crRNA (tracrRNA), and CAS9 protein, were introduced into fertilized eggs using a
445 NEPA21 super electroporator (Nepa Gene Co., Ltd, Chiba, JP). The treated eggs were
446 cultured in potassium simplex optimization medium containing amino acids (KSOMaa)
447 until the two-cell stage and were subsequently transplanted into the oviducts of 0.5-day
448 pseudopregnant ICR females. The identity of the pups was confirmed by PCR and Sanger
449 sequencing. Guide RNA and primer sequences are listed in **Table S2**.
450
451 ***In vivo* male fertility test**
452 Each 8-week-old male, carrying either the *Slc35g3* wild-type or mutated gene,
453 was individually housed with three 8-week-old B6D2F1 female mice for 2 months. Daily
454 observations were made to identify mating plugs, and the number of resultant pups was
455 recorded. A minimum of three males were included in each experimental group for
456 statistical analysis.
457
458 **Histological analysis of the testis**
459 Testes were dissected, fixed in Bouin's fluid (Polysciences, Warrington, PA,
460 USA), and embedded in paraffin wax. Subsequently, 5-µm-thick sections were obtained
461 from the paraffin blocks using a Microm HM325 microtome (Microm, Walldorf, DE,
462 Germany). The sections were sequentially dehydrated with xylene and ethanol, followed
463 by a 15-minute incubation in a 1% periodic acid solution. After washing under running
464 water for 15 min, the sections were treated with Schiff's reagent (FUJIFILM Wako,
465 Osaka, JP) for 30 min and then stained with Mayer's hematoxylin solution for 3 min after
466 an additional 15-min wash. Following these processes, the stained samples were observed
467 using SLIDEVIEW VS200 (Olympus, Tokyo, JP).
468
469 **Morphological analysis of sperm**
470 Elliptical Fourier transform analysis was performed as previously described (20,
471 21). Briefly, photographs of the spermatozoa were captured using a microscope equipped
472 with a complementary metal oxide semiconductor (CMOS) camera (BX53, DP74,
473 Olympus). The sperm head shape was manually tracked from the photographs, and the
474 elliptic Fourier analysis was performed using Momocs, a contour analysis package of the
475 statistical analysis software R x64 4.1.2(https://www.r-project.org/). Top PC1-3 scores
476 were visualized using a custom Python code.
477

478 ***In vitro* fertilization**
479 *In vitro* fertilization was performed according to the previously established
480 procedures (7). Cauda epididymal spermatozoa were dispersed in a drop of Toyoda,
481 Yokoyama, Hoshi (TYH) medium (53) covered with paraffin oil (26117-45, Nacalai
482 Tesque Inc., Kyoto, JP) for 2 h at 37°C under 5% CO_2 to facilitate capacitation. Eggs
483 obtained from the oviducts of superovulated females were placed in TYH drops.
484 Cumulus cells were removed by treating the oocytes with 330 µg/mL of hyaluronidase
485 (FUJIFILM Wako Pure Chemical Corp., Osaka, JP) for 5 min. To eliminate the ZP, eggs
486 were treated with 1 mg/mL collagenase (C1639, Merck KGaA, Darmstadt, DE,
487 Germany) for 5 min. The capacitated spermatozoa were introduced into a drop containing
488 cumulus-intact, cumulus-free, or ZP-free eggs at a final concentration of 2×10^5 or 2×10^6
489 spermatozoa/mL. Pronuclei formation was observed 8 hours after insemination.
490
491 **Computer-assisted sperm analysis**
492 Sperm velocity was analyzed as previously described (54). Cauda epididymal
493 spermatozoa were dispersed in 100 µL drops of TYH medium. Sperm motility
494 parameters were measured using the CEROS II sperm analysis system (software version
495 1.4; Hamilton Thorne Inc., Beverly, MA, USA) at 10 min and 2 h after incubation at
496 37°C under 5% CO_2. More than 200 spermatozoa were analyzed from each male.
497
498 **Assessment of sperm passage through the utero-tubal junction**
499 The assay was performed as previously described (31). Briefly, B6D2F1 female
500 mice were subjected to superovulation through intraperitoneal injection of 5 U of equine
501 chorionic gonadotropin (CG), followed by an additional 5 U of human CG (hCG) 48 h
502 later. After 12 h of hCG injection, superovulated females were placed in cages with test
503 males, and vaginal plug formation was monitored at 30-minute intervals. Upon
504 confirmation of plug formation, the males were separated from the females. After
505 approximately 2 h of plug formation, the oviducts, along with the connecting portion of
506 the uterus, were excised. These tissues were mounted on slides as whole specimens,
507 covered with coverslips, and examined using fluorescence microscopy (BZ-X810;
508 Keyence Corporation, Osaka, JP) to assess the presence of sperm containing the
509 mitochondrial DsRed2 marker.
510
511 **Plasmid construction**
512 The cDNAs encoding *mSlc35g3*, *mSlc35b2*, and *mSlc35b4* were amplified from
513 mouse testis (C57BL/6N), whereas the cDNA encoding *hSLC35G3* was amplified from a
514 human testis cDNA template (Quick Clone#637209, Takara Bio USA Inc., San Jose, CA,
515 USA). The T179HfsTer27 and F267L cDNA mutants were generated using the
516 *hSLC35G3* amplicon with the KOD Plus Mutagenesis Kit (SMK-101, TOYOBO Co.
517 LTD, Osaka, JP) following the manufacturer's protocol. The *mSlc35g3* cDNA was
518 inserted into the mCherry-tagged (C-terminus) pCAG vector, whereas the *mSlc35b2*,
519 *mSlc35b4*, *hSLC35G3*, T179HfsTer27, and F267L cDNAs were cloned into the pCAG
520 vector containing the CAG promoter and rabbit globin poly (A) signal, as previously
521 described (55). The primers used to construct these plasmids are listed in Table S2.
522
523 **Cell culture and transfection**
524 HEK293T cells (56) were cultured in DMEM (11995–065, Thermo Fisher
525 Scientific) supplemented with 10% fetal bovine serum (S1560, BioWest, Nuaillé, FR)
526 and 1% penicillin-streptomycin-glutamine (10378–016, Thermo Fisher Scientific) at

527 37°C under 5% CO_2. Subsequently, these cells were transiently transfected with the
528 plasmid DNA and cultured.
529
530 **Western blot analysis/lectin blot analysis**
531 Immunoblotting procedures closely followed those described previously
532 (57). Testis, spermatozoa from the cauda epididymis, and collected cells were immersed
533 in lysis buffer (1% Triton X-100, 50 mM Tris-HCl, pH 7.5, 150 mM NaCl) supplemented
534 with a protease inhibitor cocktail (Cat. No. 25955, Nacalai Tesque Inc.) and left to
535 incubate overnight at 4°C. To isolate testicular germ cells (TGC), the testes were minced
536 with a razor blade and passed through a 100-µm nylon mesh. Subsequently, the lysate
537 was centrifuged at 10,000 × *g* for 15 min at 4°C. The resulting supernatants were used for
538 either lectin precipitation or SDS-PAGE for immunoblot or lectin blot analysis. PNGase
539 F (P0704S, New England Biolabs Inc., Ipswich, MA, USA) was applied to the testis and
540 sperm lysates to enzymatically treat the glycosidases, following the manufacturer's
541 guidelines.
542 For lectin blot analysis, a blocking solution (10 mM Tris-HCl, 0.15 M NaCl,
543 0.05% Tween 20) was employed instead of skim milk for immunoblot analysis. The
544 primary antibody was replaced with biotin-conjugated lectin, and the secondary antibody
545 was substituted with HRP-conjugated streptavidin. The pertinent antibodies and lectins
546 are listed in Table S3.
547 For lectin precipitation, supernatants from the testis were incubated with lectin-
548 biotin overnight at 4°C, followed by incubation with streptavidin-conjugated Dynabeads
549 (Cat. No. 65001, Thermo Fisher Scientific) for 1 h at room temperature. After three
550 washes with a mild buffer (42 mM Tris-HCl, pH 7.5, 150 mM NaCl, 0.1% Triton X-100,
551 and 10% glycerol), the complexes were eluted using a sample buffer containing 2-
552 mercaptoethanol.
553
554 **Mass spectrometry**
555 The samples were subjected to mass spectrometry analysis as previously
556 described (57). "The proteins were reduced with 10 mM dithiothreitol (DTT), followed
557 by alkylation with 55 mM iodoacetamide, and digested in-gel by treatment with trypsin
558 and purified with a C18 tip (GL-Science, Tokyo, Japan). The resultant peptides were
559 subjected to nanocapillary reversed-phase LC-MS/MS analysis using a C18 column (25
560 cm × 75 µm, 1.6 µm; IonOpticks, Victoria, Australia) on a nanoLC system (Bruker
561 Daltoniks, Bremen, Germany) connected to a timsTOF Pro mass spectrometer (Bruker
562 Daltoniks) and a modified nano-electrospray ion source (CaptiveSpray; Bruker
563 Daltoniks). The mobile phase consisted of water containing 0.1% formic acid (solvent A)
564 and acetonitrile containing 0.1% formic acid (solvent B). Linear gradient elution was
565 carried out from 2% to 35% solvent B for 18 min at a flow rate of 400 nL/min. The ion
566 spray voltage was set at 1.6 kV in the positive ion mode. Ions were collected in the
567 trapped ion mobility spectrometry (TIMS) device over 100 ms, and MS and MS/MS data
568 were acquired over an m/z range of 100-1,700. During the collection of MS/MS data, the
569 TIMS cycle was adjusted to 1.1 s and included 1 MS plus 10 parallel accumulation serial
570 fragmentation (PASEF)-MS/MS scans, each containing on average 12 MS/MS spectra
571 (>100 Hz), and nitrogen gas was used as collision gas." Protein identification was carried
572 out using Mascot (version: 2.7.0; Matrix Science, London, UK) regarding
573 Scaffold_4.10.0 (Proteome Software Inc., Portland, OR, USA). Human keratin peptides
574 were excluded from the analysis.
575

Statistical analysis

Normality was assessed using the Shapiro–Wilk normality test, and variance was examined using the F-test. Non-parametric tests were performed using the Wilcoxon rank-sum test, whereas parametric tests were performed using the two-tailed Student's t-test or Welch's t-test. All statistical analyses were performed using R x64 4.1.2 (https://www.r-project.org/). Significance levels were established at *P<0.05, **P<0.01, and ***P<0.001. Data are presented as mean ± standard deviation (s.d.). Quantified data were visualized as dot plots using PlotsofData (58 https://huygens.science.uva.nl/PlotsOfData/) or custom Python code in Google Colab (https://colab.research.google.com/).

References

1. Matzuk, M.M. and Boime, I. The role of the asparagine-linked oligosaccharides of the a subunit in the secretion and assembly of human chorionic gonadotropin. J. Cell Biol. 106, 1049-1059 (1988). DOI: 10.1083/jcb.106.4.1049.
2. Matzuk, M.M., Keene, J.L., and Boime, I. Site specificity of the chorionic gonadotropin N-linked oligosaccharides in signal transduction. J. Biol. Chem. 264, 2409-2414 (1989). DOI: 10.1016/j.semcdb.2014.12.001
3. Schjoldager, K. T., Narimatsu, Y., Joshi, H. J., & Clausen, H. (2020). Global view of human protein glycosylation pathways and functions. *Nature reviews Molecular cell biology*, *21*(12), 729-749. DOI: 10.1038/s41580-020-00294-x
4. Tannous, A., Pisoni, G. B., Hebert, D. N., & Molinari, M. (2015, May). N-linked sugar-regulated protein folding and quality control in the ER. In *Seminars in cell & developmental biology* (Vol. 41, pp. 79-89). Academic Press. DOI: 10.1016/j.semcdb.2014.12.001
5. Ikawa, M., Wada, I., Kominami, K., Watanabe, D., Toshimori, K., Nishimune, Y., & Okabe, M. (1997). The putative chaperone calmegin is required for sperm fertility. *Nature*, *387*(6633), 607-611. DOI: 10.1038/42484
6. Contreras, W et al. (2022). C11orf94/Frey is a key regulator for male fertility by controlling Izumo1 complex assembly. *Science Advances*, *8*(31), eabo6049. DOI: 10.1126/sciadv.abo6049
7. Lu, Y. et al., (2023). 1700029I15Rik orchestrates the biosynthesis of acrosomal membrane proteins required for sperm–egg interaction. *Proceedings of the National Academy of Sciences*, *120*(8), e2207263120. DOI: 10.1073/pnas.2207263120
8. Tokuhiro, K., Ikawa, M., Benham, A. M., & Okabe, M. (2012). Protein disulfide isomerase homolog PDILT is required for quality control of sperm membrane protein ADAM3 and male fertility. *Proceedings of the National Academy of Sciences*, *109*(10), 3850-3855. DOI: 10.1073/pnas.1117963109
9. Oura, S., Mori, H., & Ikawa, M. (2022). Genome editing in mice and its application to the study of spermatogenesis. *Gene and Genome Editing*, *3*, 100014. DOI: 10.1016/j.ggedit.2022.100014
10. Pierre, V. et al., (2012). Absence of Dpy19l2, a new inner nuclear membrane protein, causes globozoospermia in mice by preventing the anchoring of the acrosome to the nucleus. *Development*, *139*(16), 2955-2965. DOI: 10.1242/dev.077982
11. Takasaki, N. et al., (2014). A heterozygous mutation of GALNTL5 affects male infertility with impairment of sperm motility. *Proceedings of the National Academy of Sciences*, *111*(3), 1120-1125. DOI: 10.1073/pnas.1310777111

12. Lu, Y. et al., (2019). CRISPR/Cas9-mediated genome editing reveals 30 testis-enriched genes dispensable for male fertility in mice. *Biology of Reproduction*, *101*(2), 501-511. DOI: 10.1093/biolre/ioz103
13. Raman, J., Guan, Y., Perrine, C. L., Gerken, T. A., & Tabak, L. A. (2012). UDP-N-acetyl-α-D-galactosamine: polypeptide N-acetylgalactosaminyltransferases: completion of the family tree. *Glycobiology*, *22*(6), 768-777. DOI: 10.1093/glycob/cwv003
14. Ahuja, S., & Whorton, M. R. (2019). Structural basis for mammalian nucleotide sugar transport. *Elife*, *8*, e45221. DOI: 10.7554/eLife.45221
15. J. Ruan et al., TreeFam: 2008 update. *Nucleic Acids Res.* **36**(suppl_1), D735–D740 (2007). DOI: 10.1093/nar/gkm1005
16. M. J. Robertson, et al., Large-scale discovery of male reproductive tract-specific genes through analysis of RNA-seq datasets. *BMC Biol*. **18**(1), 103 (2020). DOI: 10.1186/s12915-020-00826-z
17. R. Wang et al., Construction of a cross-species cell landscape at single-cell level. *Nucleic Acids Res.* **51**(1), 501–516 (2022). DOI: 10.1093/nar/gkac633
18. J. Jumper et al., Highly accurate protein structure prediction with AlphaFold. *Nature* **596**, 583–589 (2021). DOI: 10.1038/s41586-021-03819-2
19. K. D. Tsirigos, C. Peters, N. Shu, L. Käll, A. Elofsson, The TOPCONS web server for consensus prediction of membrane protein topology and signal peptides. *Nucleic Acids Res*. **43**(W1), W401–W407 (2015). DOI: 10.1093/nar/gkv485
20. F. P. Kuhl, C. R. Giardina, Elliptic Fourier features of a closed contour. *Comput. Graph. Image Process.* **18**(3), 236–258 (1982).
21. D. Mashiko, M. Ikawa, K. Fujimoto, Mouse spermatozoa with higher fertilization rates have thinner nuclei. *PeerJ* **5**, e3913 (2017). DOI: 10.7717/peerj.3913
22. A. Morohoshi, H. Miyata, Y. Oyama, S. Oura, T. Noda, M. Ikawa, FAM71F1 binds to RAB2A and RAB2B and is essential for acrosome formation and male fertility in mice. *Development* **148**(21), dev199644 (2021). DOI: 10.1242/dev.199644
23. H. Hasuwa, Y. Muro, M. Ikawa, N. Kato, Y. Tsujimoto, M. Okabe, Transgenic mouse sperm that have green acrosome and red mitochondria allow visualization of sperm and their acrosome reaction in vivo. *Exp. Anim.* **59**(1), 105–107 (2010). DOI: 10.1538/expanim.59.105
24. Y. N. Lin, A. Roy, W. Yan, K. H. Burns, M. M. Matzuk, Loss of zona pellucida binding proteins in the acrosomal matrix disrupts acrosome biogenesis and sperm morphogenesis. *Mol. Cell Biol.* **27**(19), 6794–6805 (2007). DOI: 10.1128/MCB.01029-07
25. R. Yao, C. Ito, Y. Natsume, Y. Sugitani, H. Yamanaka, S. Kuretake, K. Yanagida, A. Sato, K. Toshimori, T. Noda, Lack of acrosome formation in mice lacking a Golgi protein, GOPC. *Proc. Natl. Acad. Sci. U. S. A.* **99**, 11211–11216 (2002). DOI: 10.1073/pnas.162027899
26. Y. Fujihara, Y. Satouh, N. Inoue, A. Isotani, M. Ikawa, M. Okabe, SPACA1-deficient male mice are infertile with abnormally shaped sperm heads reminiscent of globozoospermia. *Development* **139**(19), 3583–3589 (2012). DOI: 10.1242/dev.081778
27. E. Kim, M. Yamashita, T. Nakanishi, K. E. Park, M. Kimura, S. I. Kashiwabara, T. Baba, Mouse sperm lacking ADAM1b/ADAM2 fertilin can fuse with the egg plasma membrane and effect fertilization. *J. Biol. Chem.* **281**(9), 5634–5639 (2006). DOI: 10.1074/jbc.M510558200

670 28. Y. Fujihara, A. Oji, K. Kojima-Kita, T. Larasati, M. Ikawa, Co-expression of sperm
671 membrane proteins CMTM2A and CMTM2B is essential for ADAM3 localization and
672 male fertility in mice. *J. Cell Sci.* **131**(19), jcs221481 (2018). DOI: 10.1242/jcs.221481
673 29. R. Shamsadin, I. M. Adham, K. Nayernia, U. A. Heinlein, H. Oberwinkler, W. Engel,
674 Male mice deficient for germ-cell cyritestin are infertile. *Biol. Reprod.* **61**(6), 1445–
675 1451 (1999). DOI: 10.1095/biolreprod61.6.1445
676 30. R. Yamaguchi, Y. Muro, A. Isotani, K. Tokuhiro, K. Takumi, I. Adham, M. Ikawa, M.
677 Okabe, Disruption of ADAM3 impairs the migration of sperm into oviduct in mouse.
678 *Biol. Reprod.* **81**(1), 142–146 (2009). DOI: 10.1095/biolreprod.108.074021
679 31. Y. Fujihara, K. Tokuhiro, Y. Muro, G. Kondoh, Y. Araki, M. Ikawa, M. Okabe,
680 Expression of TEX101, regulated by ACE, is essential for the production of fertile
681 mouse spermatozoa. *Proc. Natl. Acad. Sci.* **110**(20), 8111–8116 (2013). DOI:
682 10.1073/pnas.1222166110
683 32. J. H. Krege, S. W. John, L. L. Langenbach, J. B. Hodgin, J. R. Hagaman, E. S.
684 Bachman, J. C. Jennette, D. A. O'Brien, O. Smithies, Male-female differences in
685 fertility and blood pressure in ACE-deficient mice. *Nature* **375**,146–148 (1995). DOI:
686 10.1038/375146a0.
687 33. J. R. Hagaman, J. S. Moyer, E. S. Bachman, M. Sibony, P. L. Magyar, J. E. Welch, O.
688 Smithies, J. H. Krege, D. A. O'Brien, Angiotensin-converting enzyme and male
689 fertility. *Proc. Natl. Acad. Sci. U. S. A.* **95**, 2552–2557 (1998). DOI:
690 10.1073/pnas.95.5.2552.
691 34. R. Yamaguchi, K. Yamagata, M. Ikawa, S. B. Moss, M. Okabe, Aberrant distribution of
692 ADAM3 in sperm from both angiotensin-converting enzyme (Ace)—and calmegin
693 (Clgn)-deficient mice. *Biol. Reprod.* **75**, 760–766 (2006). DOI:
694 10.1095/biolreprod.106.052977
695 35. Y. Fujihara, M. Okabe, M. Ikawa, GPI-anchored protein complex, LY6K/TEX101, is
696 required for sperm migration into the oviduct and male fertility in mice. *Biol. Reprod.*
697 **90**(3), 60–61 (2014). DOI: 10.1095/biolreprod.113.112888
698 36. Y. Fujihara, S. Herberg, A. Blaha, K. Panser, K. Kobayashi, T. Larasati, M.
699 Novatchkova, H. C. Theussl, O. Olszanska, M. Ikawa, A. Pauli, The conserved fertility
700 factor SPACA4/Bouncer has divergent modes of action in vertebrate fertilization. *Proc.*
701 *Natl. Acad. Sci. U. S. A*. **118**(39), e2108777118 (2021). DOI: 10.1073/pnas.2108777118
702 37. Y. Fujihara, T. Noda, K. Kobayashi, A. Oji, S. Kobayashi, T. Matsumura, T. Larasati,
703 S. Oura, K. Kojima-Kita, Z. Yu, M. M. Matzuk, M. Ikawa, Identification of multiple
704 male reproductive tract-specific proteins that regulate sperm migration through the
705 oviduct in mice. *Proc. Natl. Acad. Sci. U. S. A.* **116**(37), 18498–18506 (2019). DOI:
706 10.1073/pnas.1908736116
707 38. N. Inoue, M. Ikawa, A. Isotani, M. Okabe, The immunoglobulin superfamily protein
708 Izumo is required for sperm to fuse with eggs. *Nature* **434**(7030), 234–238
709 (2005). DOI: 10.1038/nature03362
710 39. K. Toshimori, S. Araki, I. Tanii, C. Ōura, Masking the cryptodeterminant on the 54-
711 kilodalton mouse sperm surface antigen. *Biol. Reprod.* **47**(6), 1161–1167 (1992). DOI:
712 10.1095/biolreprod47.6.1161
713 40. T. Noda, Y. Lu, Y. Fujihara, S. Oura, T. Koyano, S. Kobayashi, M. M. Matzuk, M.
714 Ikawa, Sperm proteins SOF1, TMEM95, and SPACA6 are required for sperm− oocyte
715 fusion in mice. *Proc. Natl. Acad. Sci. U. S. A.* **117**(21), 11493–11502 (2020). DOI:
716 10.1073/pnas.1922650117
717 41. D. Bojar, L. Meche, G. Meng, W. Eng, D. F. Smith, R. D. Cummings, L. K. Mahal, A
718 useful guide to lectin binding: machine-learning directed annotation of 57 unique lectin

specificities. *ACS Chem. Biol.* **17**(11), 2993–3012 (2022). DOI: 10.1021/acschembio.1c00689

42. S. Chen, L.C. Francioli, J.K. Goodrich et al. A genomic mutational constraint map using variation in 76,156 human genomes. Nature 625, 92–100 (2024). DOI: 10.1038/s41586-023-06045-0
43. J. Cheng, G. et al., Accurate proteome-wide missense variant effect prediction with AlphaMissense. *Science* **381**(6664), eadg7492 (2023). DOI: 10.1126/science.adg7492
44. I. A. Adzhubei, S. Schmidt, L. Peshkin, V. E. Ramensky, A. Gerasimova, P. Bork, A. S. Kondrashov, S. R. Sunyaev. A method and server for predicting damaging missense mutations, *Nat Methods* **7**(4), 248–249 (2010). DOI: 10.1038/nmeth0410-248
45. JM. Bedford . Effects of elevated temperature on the epididymis and testis: experimental studies. Adv Exp Med Biol. 1991;286:19-32. DOI: 10.1007/978-1-4684-5913-5_3.
46. M. Aebi, N-linked protein glycosylation in the ER. *Biochim. Biophys. Acta* **1833**(11), 2430–2437 (2013). DOI: 10.1016/j.bbamcr.2013.04.001
47. Wang, H., Iida-Norita, R., Mashiko, D., Pham, A. H., Miyata, H., & Ikawa, M. (2024). Golgi associated RAB2 interactor protein family contributes to murine male fertility to various extents by assuring correct morphogenesis of sperm heads. *PLoS Genetics*, *20*(6), e1011337. DOI: 10.1371/journal.pgen.1011337
48. Martinez, G. et al., (2022). Oligogenic heterozygous inheritance of sperm abnormalities in mouse. *Elife*, *11*, e75373. DOI: 10.7554/eLife.75373
49. Fujihara, Y., Miyata, H., & Ikawa, M. (2018). Factors controlling sperm migration through the oviduct revealed by gene-modified mouse models. *Experimental Animals*, *67*(2), 91-104. DOI: 10.1538/expanim.17-0153
50. D. Wang, L. Cheng, W. Xia, X. Liu, Y. Guo, X. Yang, X. Guo, E. Y. Xu, LYPD4, mouse homolog of a human acrosome protein, is essential for sperm fertilizing ability and male fertility. *Biol. Reprod.* **102**(5), 1033–1044 (2020). DOI: 10.1093/biolre/ioaa018
51. N. Inoue, M. Ikawa, M. Okabe, Putative sperm fusion protein IZUMO and the role of N-glycosylation. *Biochem. Biophys. Res. Commun.* **377**, 910–914 (2008). DOI: 10.1016/j.bbrc.2008.10.073
52. Kotaja, N. et al., (2004). Preparation, isolation and characterization of stage-specific spermatogenic cells for cellular and molecular analysis. *Nature methods*, *1*(3), 249-254. DOI: 10.1038/nmeth1204-249
53. Y. Toyoda, M. Yokoyama, T. Hosi, Studies on the fertilization of mouse eggs in vitro. *Jpn. J. Anim. Reprod.* **16**, 152–157 (1971). DOI: 10.1262/jrd1955.16.152
54. H. Miyata, Y. Satouh, D. Mashiko, M. Muto, K. Nozawa, K. Shiba, Y. Fujihara, A. Isotani, K. Inaba, M. Ikawa, Sperm calcineurin inhibition prevents mouse fertility with implications for male contraceptive. *Science*, **350**(6259), 442–445 (2015). DOI: 10.1126/science.aad0836
55. H. Niwa, K. Yamamura, J. Miyazaki, Efficient selection for high-expression transfectants with a novel eukaryotic vector. *Gene* **108**, 193–199 (1991). DOI: 10.1016/0378-1119(91)90434-d
56. G. Tiscornia, O. Singer, I. M. Verma, Production and purification of lentiviral vectors. *Nat. Protoc.* **1**, 241–245 (2006). DOI: 10.1038/nprot.2006.37
57. K. Shimada, S. Park, H. Miyata, Z. Yu, A. Morohoshi, S. Oura, M. M. Matzuk, M. Ikawa, ARMC12 regulates spatiotemporal mitochondrial dynamics during spermiogenesis and is required for male fertility. *Proc. Natl. Acad. Sci. U. S. A.* **118**, e2018355118 (2021). DOI: 10.1073/pnas.2018355118

58. M. Postma, J. Goedhart, PlotsOfData—A web app for visualizing data together with their summaries. *PLoS Biol.* **17**(3), e3000202 (2019). DOI: 10.1371/journal.pbio.3000202

Acknowledgments

We express our sincere gratitude to Ms. Saki Nishioka and the NPO for Biotechnology Research and Development for their valuable technical support and to the members of both the Department of Experimental Genome Research and Animal Resource Center for Infectious Diseases at the Research Institute for Microbial Diseases (RIMD) of Osaka University, Japan for their assistance and engaging discussions during the experiments. We acknowledge the RIMD NGS core facility for its valuable support in sequencing and data analysis. We also thank A. Ninomiya and F. Sugihara for MS analysis (RIMD Core Instrumentation Facility).

Funding: This work was financially supported by the Ministry of Education, Culture, Sports, Science and Technology/Japan Society for the Promotion of Science (JP21K19569 and JP22H03214 to H.M.; JP21H05033, JP22H04922 and JP23K20043 to M.I.); the Japan Science and Technology Agency (JPMJFR211F to H.M.; JPMJCR21N1 to M.I.); the Japan Agency for Medical Research and Development (JP23jf0126001, JP23fa627002, and JP23fa627006 to M.I.); the Takeda Science Foundation (grants to H.M. and M.I.); the *Eunice Kennedy Shriver* National Institute of Child Health and Human Development (R01HD088412 to M.M and M.I.); and the Bill & Melinda Gates Foundation (INV-001902 to M.M. and M.I.). OU master plan (JPMXP1323015484 to M.I.)

Data and material availability: All data needed to evaluate the conclusions in the paper are present in the paper and/or the Supplementary Materials. The gene-manipulated mouse lines used in this study were deposited at the RIKEN BioResource Research Center (RIKEN BRC, Tsukuba, Japan) and the Center for Animal Resources and Development (CARD), Kumamoto University (Kumamoto, Japan). These cell lines are available through these centers, subject to scientific review and completion of a material transfer agreement. Requests for access to genetically manipulated mice should be submitted to these centers.

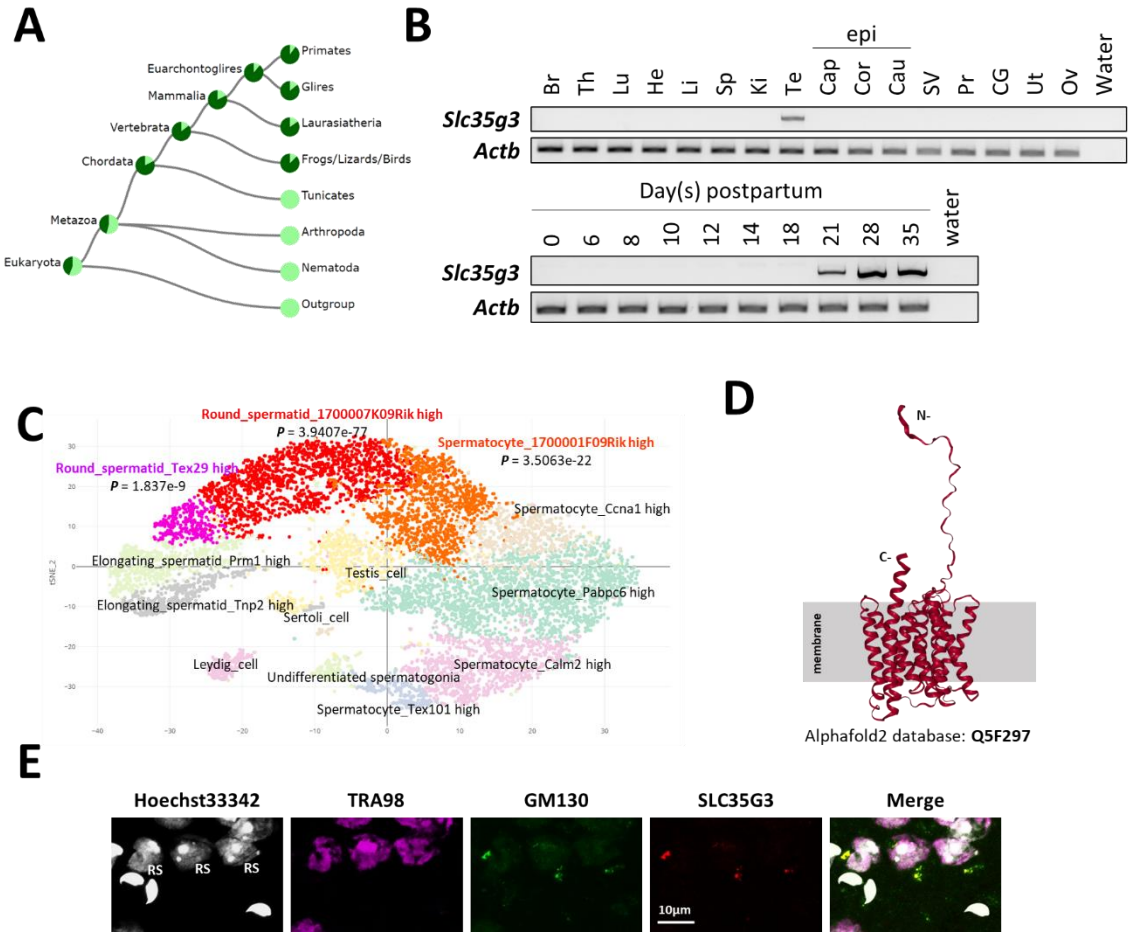

Fig. 1. SLC35G3 is a multi-pass transmembrane protein with unique testes-specific expression in the Golgi apparatus during early spermiogenesis.
(A) Phylogenetic tree of *Slc35g3* from the TreeFam database, with dark green areas indicating the presence and light green areas indicating the absence of *Slc35g3*. **(B)** RT-PCR results across multiple tissues (upper panel) and from testes at various days postpartum (lower panel); Br: brain, Th: thymus, Lu: lung, He: heart, Li: liver, Sp: spleen, Ki: kidney, Te: testis; Epi: epididymis, Cap: caput epididymis, Cor: corpus epididymis, Cau: cauda epididymis; SV: seminal vesicle, Pr: prostate, CG: coagulating gland, Ut: uterus, Ov: ovary. β-actin (Actb) was used as the loading control. **(C)** scRNA-seq prediction of cells strongly expressing *Slc35g3* mRNA (Mouse cell atlas). Dots with low transparency represent cells with predicted expression. **(D)** SLC35G3 structure predicted using AlphaFold. **(E)** From left to right: Hoechst33342 staining image, SLC35G3 immunostaining image, GM130 immunostaining image, and merged image of wild-type testicular germ cells. Scale bar: 10 μm, RS: Round Spermatid

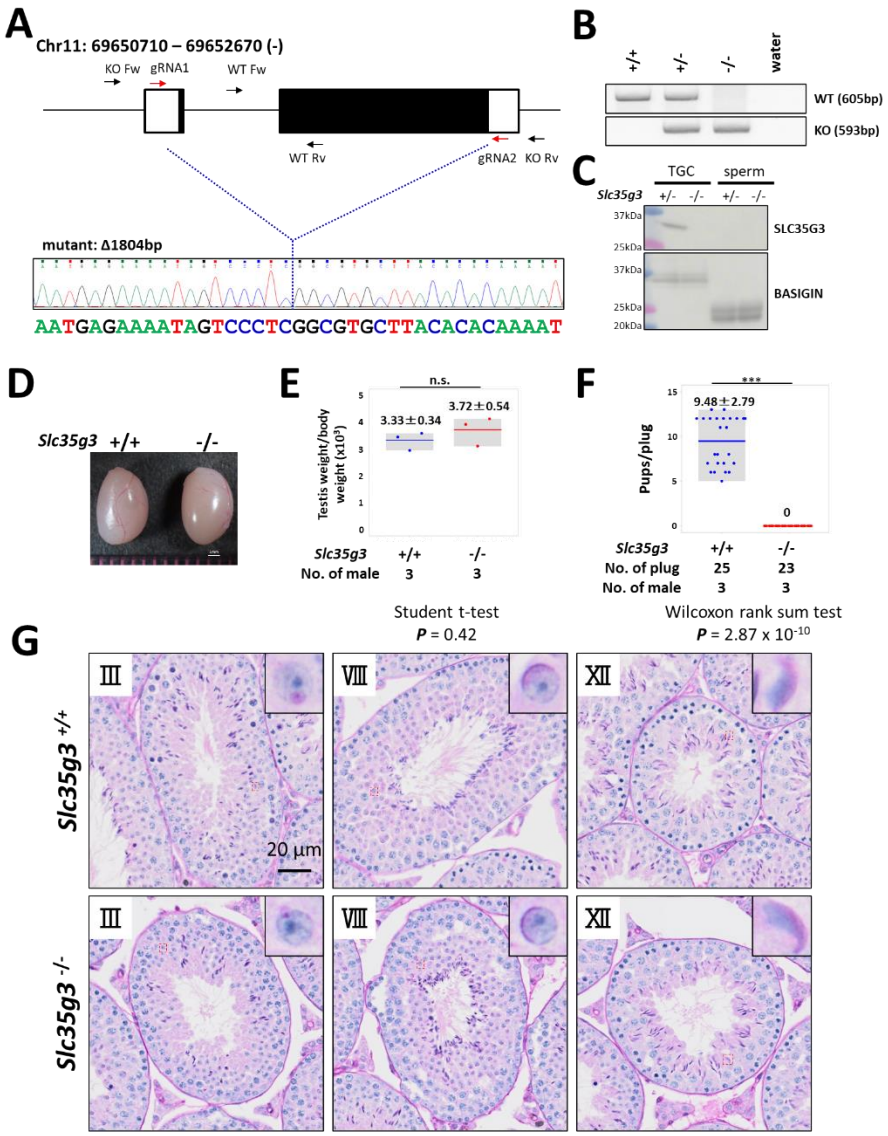

Fig. 2. *Slc35g3*$^{-/-}$ induces male sterility.

(A) Depiction of *Slc35g3* gene location and structure, gRNA/primer design, and the sequencing result of the mutant (deleted) allele. **(B)** PCR genotyping results for *Slc35g3*$^{+/+}$, *Slc35g3*$^{+/-}$, *Slc35g3*$^{-/-}$, and water are presented. **(C)** Western blot analysis results obtained with *Slc35g3*$^{+/-}$ and *Slc35g3*$^{-/-}$ testicular germ cells (TGC) lysates and *Slc35g3*$^{+/-}$ and *Slc35g3*$^{-/-}$-derived cauda epididymal sperm lysates are shown. **(D, E)** Similar testis sizes (D) and weights (E) from *Slc35g3*$^{+/+}$ and *Slc35g3*$^{-/-}$ mice (two-sided Student's t-test; $P = 0.42$). **(F)** Comparison of the number of pups per vaginal plug between *Slc35g3*$^{+/+}$ and *Slc35g3*$^{-/-}$ mice (Wilcoxon rank-sum test; $P = 2.87 \times 10^{-10}$. **(G)** Histological analysis of testis sections from *Slc35g3*$^{+/+}$ mice (upper panels) and those from *Slc35g3*$^{-/-}$ mice (lower panels); images depict stages III (Golgi phase), VIII (acrosome phase), and XII (maturation phase).

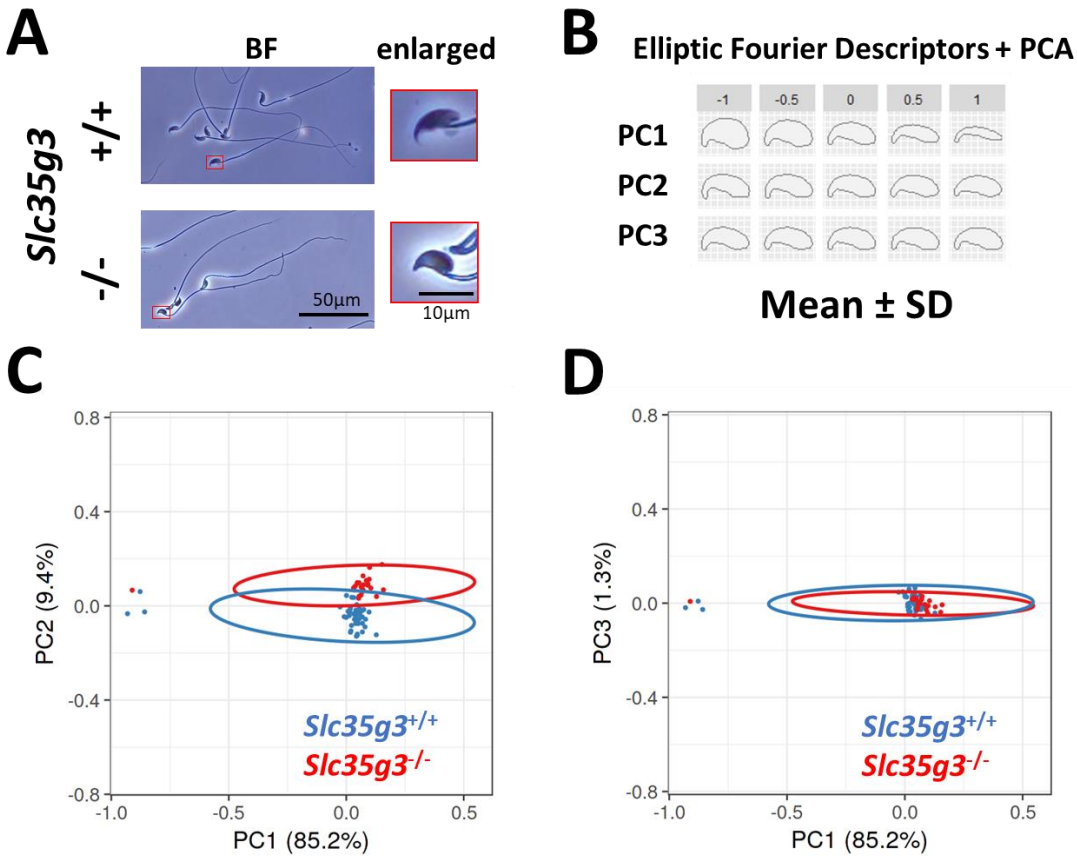

Fig. 3. *Slc35g3* is involved in the regulation of sperm head morphology
(A) Bright-field (BF) views of *Slc35g3*$^{+/+}$-derived sperm (upper panels) versus *Slc35g3*$^{-/-}$-derived sperm (lower panels); red frames are images enlarged four times. Scale bar: 50 µm for BF images, 10 µm for enlarged ones. **(B)** Morphological characteristics are indicated by mean ± SD of each principal component (PC) following elliptic Fourier analysis; the upper value represents SD, with zero indicating average morphology. **(C, D)** Plots of PC1-PC2 (C) and PC1-PC3 (D) coordinates of the elliptic Fourier analysis of sperm from *Slc35g3*$^{+/+}$ mice (blue encircled) versus *Slc35g3*$^{-/-}$ mice (red encircled); circles represent 95% confidence ellipses. Scale bar = 10 µm.

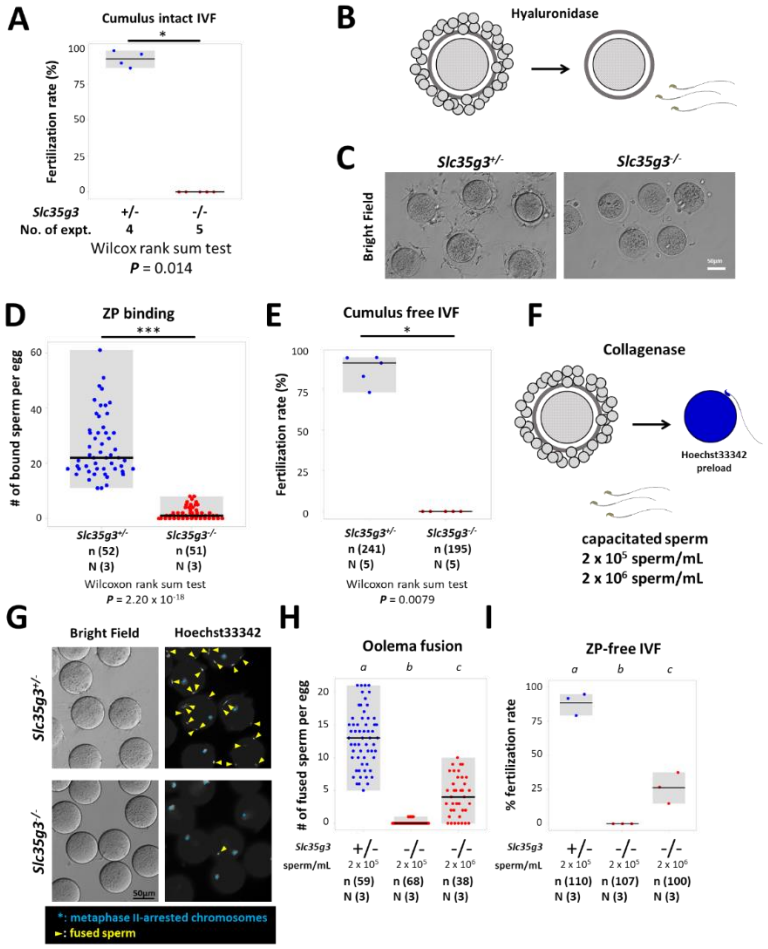

Fig. 4. *Slc35g3*$^{-/-}$-derived spermatozoa are defective in ZP binding and oolemma fusion.

(A) The IVF fertilization rate of cumulus-intact oocytes using *Slc35g3*$^{+/-}$ and *Slc35g3*$^{-/-}$ -derived sperm. Wilcoxon rank-sum test $P = 0.014$. (B) Outline of the procedure of cumulus cell-free IVF. (C) *Slc35g3*$^{+/-}$-derived and *Slc35g3*$^{-/-}$-derived sperm binding to cumulus-free oocytes after insemination. Scale bar = 50 µm. (D) The number of bound sperm per egg for *Slc35g3*$^{+/-}$-derived and *Slc35g3*$^{-/-}$-derived sperm (Wilcoxon rank-sum test $P = 2.20 \times 10^{-18}$). (E) The fertilization rate of cumulus cell-free IVF using Slc35g3$^{+/-}$-derived and Slc35g3$^{-/-}$-derived sperm. (F) The procedure of ZP-free IVF. Wilcoxon rank-sum test; $\boldsymbol{P} = 0.0079$. (G) Brightfield and Hoechst33342 staining of oocytes and *Slc35g3*$^{+/-}$-derived and *Slc35g3*$^{-/-}$-derived sperm after insemination into ZP-free oocytes; Yellow arrowheads indicate fused spermatozoa and light blue asterisks indicate metaphase II-arrested chromosomes. (H) The number of fused sperm per egg using *Slc35g3*$^{+/-}$-derived and *Slc35g3*$^{-/-}$-derived sperm (2×10^5 sperm/mL and 2×10^6 sperm/mL, respectively). Significant differences are indicated by distinct symbols. (I) The fertilization rate of ZP-free IVF using *Slc35g3*$^{+/-}$-derived and *Slc35g3*$^{-/-}$-derived sperm (2×10^5 sperm/mL and 2×10^6 sperm/mL, respectively). Significant differences are indicated by distinct symbols.

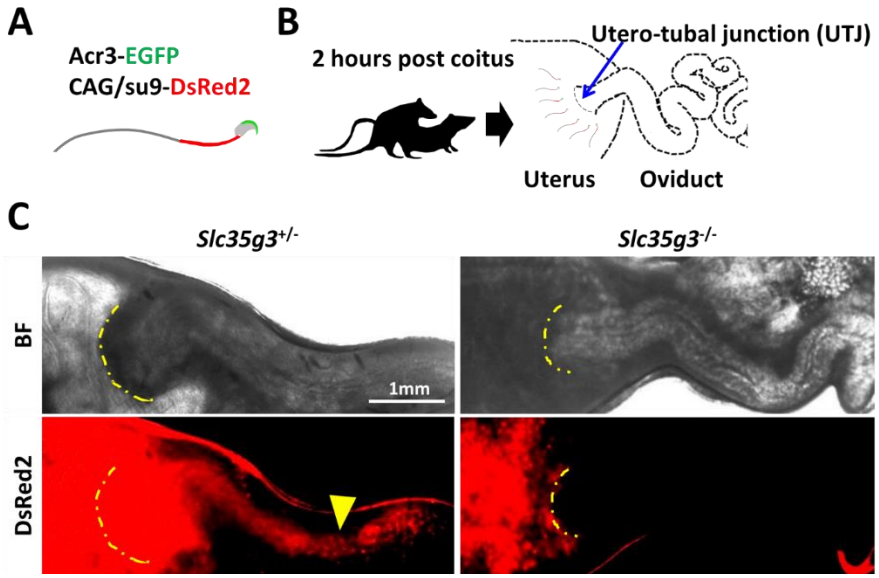

Fig. 5. *Slc35g3*-deficient mice show impaired sperm migration to the oviduct
(A) Illustration of Tg (CAG/su9-DsRed2, Acr3-eGFP) sperm. **(B)** A schematic diagram of the sperm migration assay. **(C)** Bright field (top panel) and Dsred2 (bottom panel) images of the uteri and oviducts of females after mating with control *Slc35g3*$^{+/-}$and *Slc35g3*$^{-/-}$ male mice. The yellow dashed line indicates the uterotubal junction (UTJ), and the yellow arrowhead represents the sperm from control *Slc35g3*$^{+/-}$ male mice that have traversed the UTJ.

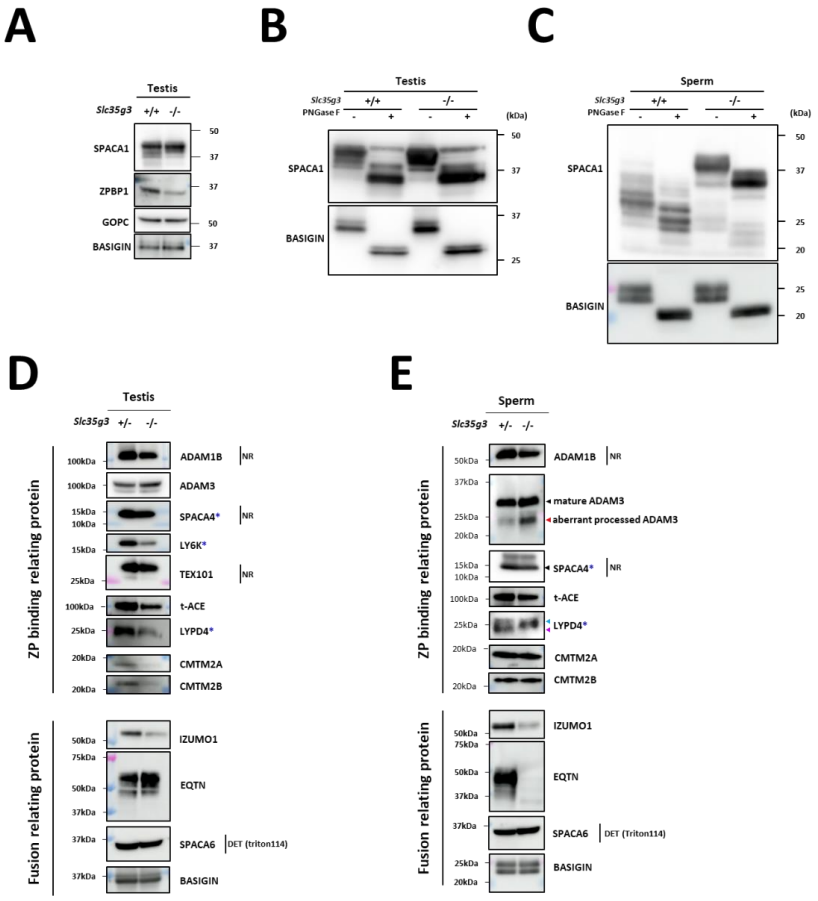

Fig. 6. Disruption of *Slc35g3* leads to its reduced testicular expression and abnormal processing of multiple sperm proteins

(A) Western blot analyses of SPACA1, ZPBP1, and GOPC in *Slc35g3*$^{+/+}$ and *Slc35g3*$^{-/-}$ testes, with BASIGIN used as a loading control. **(B)** Western blot analysis of PNGaseF-treated or non-treated SPACA1 in *Slc35g3*$^{+/+}$ and *Slc35g3*$^{-/-}$ testes, with BASIGIN used as a loading control. **(C)** Western blot analysis of PNGaseF-treated or non-treated SPACA1 in *Slc35g3*$^{+/+}$-derived and *Slc35g3*$^{-/-}$-derived spermatozoa, with BASIGIN used as a loading control. **(D)** Western blot analyses of ADAM1B, ADAM3, SPACA4, LY6K, TEX101, t-ACE, LYPD4, CMTM2A, CMTM2B, IZUMO1, EQTN, and SPACA6 in *Slc35g3*$^{+/-}$ and *Slc35g3*$^{-/-}$ testes, with BASIGIN used as a loading control. All protein samples were processed under reducing and denaturing conditions unless otherwise specified. Non-reducing and non-denaturing conditions are denoted as NR. For SPACA6 detection, fractions of testis proteins from wild-type and knockout specimens, extracted using Triton X-114, were utilized (abbreviated as DET). Genes marked with blue asterisks show reduced ZP binding upon knockout, whereas ADAM3 remains unaffected. **(E)** Western blot analyses of ADAM1B, ADAM3, SPACA4, t-ACE, LYPD4, CMTM2A, CMTM2B, IZUMO1, EQTN, and SPACA6 in *Slc35g3*$^{+/+}$-derived and *Slc35g3*$^{-/-}$-derived spermatozoa, BASIGIN used as a loading control. The black arrowhead indicates the predicted protein size, whereas the red arrowhead indicates an aberrantly processed protein isoform. Additionally, the light blue and purple arrowheads mark the two bands observed in the wild-type sample.

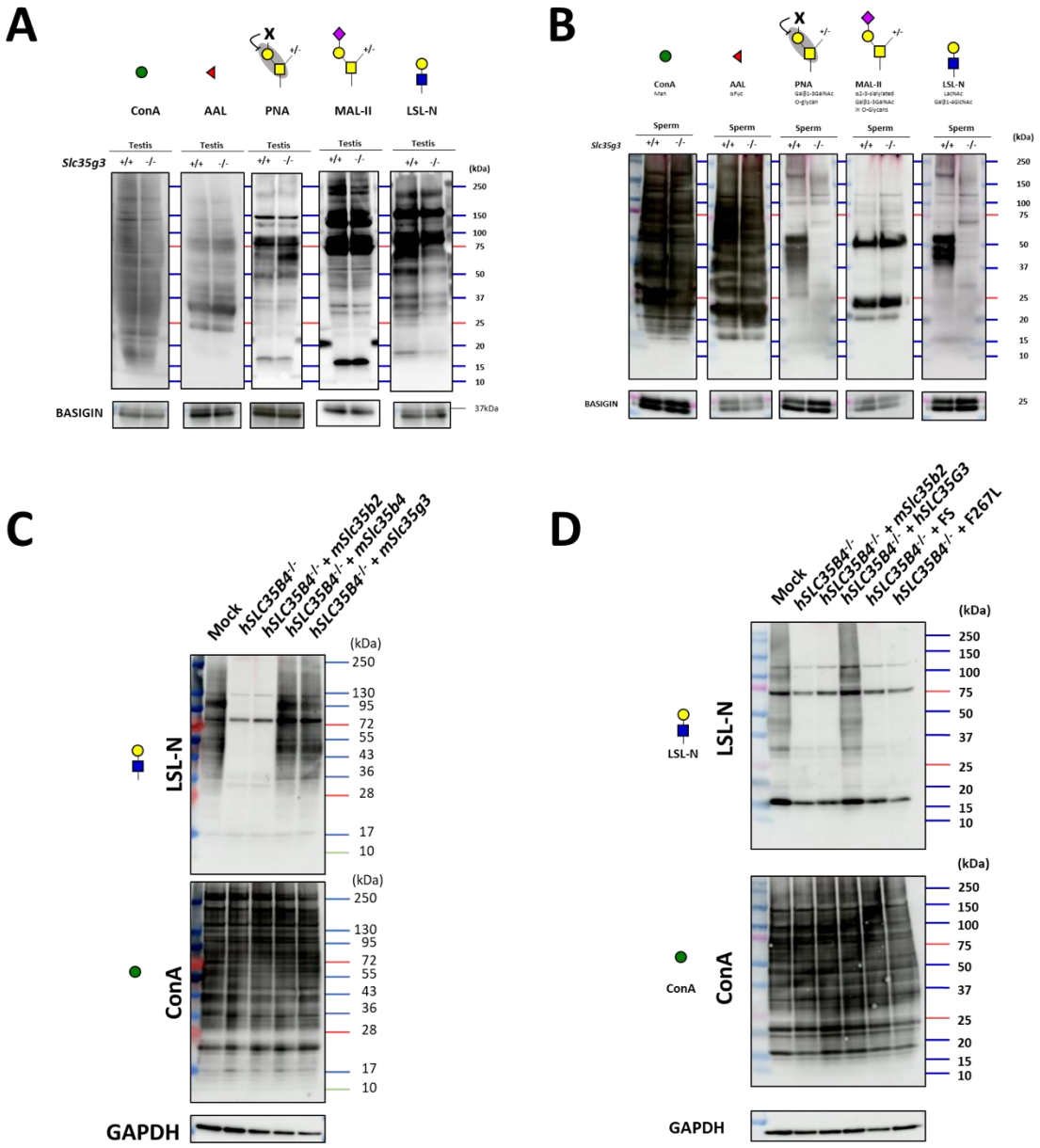

Fig. 7. *Slc35g3*$^{-/-}$ testis showed impaired glycan structure

(A) Lectin blot (LB) analyses using ConA, AAL, PNA, MAL-II, and LSL-N in *Slc35g3*$^{+/+}$ and *Slc35g3*$^{-/-}$ testes, BASIGIN as a loading control. Green circles represent mannose, red triangles fucose, yellow squares GalNAc, yellow circles galactose, purple diamonds sialic acid, and blue squares GlcNAc. **(B)** LB analyses using ConA, AAL, PNA, MAL-II, and LSL-N in *Slc35g3*$^{+/+}$ and *Slc35g3*$^{-/-}$ derived spermatozoa. **(C)** LB analyses of LSL-N and ConA in SLC35B4-deficient HEK293T cells, with GAPDH as a loading control. mSlc35b2, mSlc35b4 and mSlc35g3 were expressed in SLC35B4 deficient cells. **(D)** LB analyses of LSL-N and ConA in hSLC35G3 mutant transfected SLC35B4 deficient cells, with GAPDH, were used as a loading control. FS: T179HfsTer27.